RSC Advances

PAPER

View Article Online
View Journal | View Issue

Check for updates

Cite this: *RSC Adv.*, 2020, **10**, 35873

# Organic–inorganic hybrid liquid crystals of azopyridine-enabled halogen-bonding towards sensing in aquatic environment†

Yinjie Chen,[a] Luhai Li,[a] Yonggang Yang,[a] Hari Krishna Bisoyi,[b] Yunling Jia,[c] Jing Ju,[c] Shuai Huang,[d] Haifeng Yu,*[e] Huai Yang*[e] and Quan Li*[b]

Received 8th August 2020
Accepted 4th September 2020

DOI: 10.1039/d0ra06838a

rsc.li/rsc-advances

In this study, organic–inorganic hybrid mesogens of silver nanoparticles (Ag NPs) and azopyridines (AzoPys) enabled by halogen bonding were prepared. Triple functions of the degree of orientation change, metal-enhanced fluorescence, and surface-enhanced Raman scattering were observed in Ag···Br–Br···AzoPy nanoparticles (12Br–Ag), which were induced by the *in situ* synthesis of Ag NPs in AzoPy. The bromine molecules were then linked by halogen bonding and electrostatic interaction resulting in the smectic A phase of 12Br–Ag. To demonstrate the potential of Br–Br···AzoPy (12Br) as a practical sensor, we used the 12Br compound to detect silver in an aqueous condition, and significant signals of the halogen-bonded complex-silver system were observed in the X-ray diffraction pattern and Raman spectra. Herein, we provide a novel perspective and design principle for the practical applications of organic–inorganic hybrid liquid crystals in environmental monitoring.

Open Access Article. Published on 30 September 2020. Downloaded on 7/18/2025 9:02:30 PM.
This article is licensed under a Creative Commons Attribution-NonCommercial 3.0 Unported Licence.

Halogen bonding is an attractive intermolecular interaction for adjusting the interaction strength by choosing suitable halogen atoms that participate in the bond formation without significantly changing the electronic structure of the compound.[1] Azobenzene-containing composites are of great interest, having promising applications in various fields, such as, optical data storage, owing to the reversible *trans–cis* photoisomerisation of azobenzene chromophores.[2–5] The halogen-bonded liquid crystals of azobenzene were first reported in 2012.[6] Currently, many studies describe halogen bonding using azobenzene in the field of organic-liquid crystals[7,8] and photoresponsive nanocomposites;[9–12] however, few studies have investigated the metal-containing azobenzene mesogens. Recently, azobenzene hybrid mesogen-capped thiolated ligands of gold and silver nanoparticles with lamellar and columnar superstructures were achieved and changed the phase transitions significantly; they can behave as intriguing photo-switched temperature sensors with storage and erase functionality with well-organised hybrid systems.[13] The coupling of the azobenzene mesogen with inorganic nanoparticles has recently become an attractive approach as it can give rise to novel hybrid materials in which the properties of the two components are mutually enhanced.[14] However, studies have not explored organic–inorganic hybrid liquid crystals of azobenzene-containing composites with intermolecular interactions for this purpose, not to mention exploring their applications for the next generation of liquid crystal sensors.

Herein, we report azopyridine (AzoPy) mesogens embedded with silver nanoparticles (Ag NPs) obtained by halogen-bonding. Although the texture or degree of orientation remained unchanged in Ag···Br–Br···AzoPy (12Br–Ag) compared to that in Br–Br···AzoPy (12Br), a clear birefringence change was detected, which was attributed to the variation in the electronic properties of 12Br–Ag with a shorter *d*-spacing. Meanwhile, the halogen bonding intensified the metal-enhanced fluorescence (MEF) of the AzoPy ligand by inserting $Br_2$ between the Ag NPs and ligand molecules in the solution along with the Surface-enhanced Raman (SER) scattering but not in the condensed phases (crystal or mesophase). By taking advantage of the assisted enhancement of MEF and SER factors of halogen bonding, we report a new approach for the sewage detection by identifying the trace metals using a halogen-bonded liquid crystal as a sensor in water owing to its high sensitivity; it may possess the potential to transform the waste metal pollution into treasure.

[a]*Beijing Engineering Research Center of Printed Electronics, Beijing Institute of Graphic Communication, Beijing 102600, China*

[b]*Advanced Materials and Liquid Crystal Institute and Chemical Physics Interdisciplinary Program, Kent State University, Kent, OH 44242, USA. E-mail: quanli3273@gmail.com*

[c]*College of Chemistry and Molecular Engineering, Peking University, Beijing 100871, China*

[d]*Southeast University, Chemistry and Chemical Engineering, Nanjing, Jiangsu, CN 211189, China*

[e]*Department of Materials Science and Engineering, Peking University, Beijing 100871, China. E-mail: yuhaifeng@pku.edu.cn; yanghuai@pku.edu.cn*

† Electronic supplementary information (ESI) available. See DOI: 10.1039/d0ra06838a

Open Access Article. Published on 30 September 2020. Downloaded on 7/18/2025 9:02:30 PM.
This article is licensed under a Creative Commons Attribution-NonCommercial 3.0 Unported Licence.

The organic–inorganic hybrid liquid crystals of azopyridines are shown in Scheme 1. Generally, there are two approaches for preparing nanoparticles: *ex situ* and *in situ* (direct growth). The *in situ* synthesis induces the morphology-controlled growth of nanoparticles.[15,16] Thus, we adopted the *in situ* synthesis of Ag NPs (10 wt%) with the ligand AzoPy, followed by a treatment with molecular $Br_2$ to obtain the organic–inorganic hybrid liquid crystals of Ag NPs and AzoPy. The synthesis protocols are given in the ESI.† The resulting Ag···Br–Br···AzoPy nanoparticles were characterized by scanning transmission electron microscopy (STEM), energy dispersive spectroscopy (EDS), transmission electron microscopy (TEM), powder X-ray diffraction (XRD), UV-vis absorption, and Raman spectroscopy.

The STEM, TEM, and EDS elemental mapping were performed on the hybrid Ag NPs. As shown in Fig. 1(a), the Ag NPs were covered by an organic corona of the halogen-bonded complex Br–Br···AzoPy, which is a result of the interactions between Ag NPs and a pyridyl moiety in AzoPy linked molecular $Br_2$ by halogen bonding and electrostatic interactions. Moreover, the EDS mapping data support the presence of Ag and Br atoms in the hybrid nanoparticles (Fig. 1(b)). Fig. 1(c) shows an organic layer surrounding the Ag NPs with a small thickness, and the EDS mapping demonstrates the presence of Ag (Fig. 1(d)) and Br (Fig. 1(e)) in the hybrid nanoparticles. The HR-TEM images also showed distinct lattice fringe patterns, indicating the highly crystalline nature of the Ag nanocrystals. The obtained lattice spacing was 0.25 nm, which agrees with the (111) plane for the face-centred cubic (fcc) crystal structure of bulk Ag.[17] The collective EDS mapping and STEM/TEM results provide a definitive evidence for the stabilised halogen-bonded complex of Ag NPs. However, a structure of Ag···AzoPy nanoparticles devoid of halogen bonding was not identified (Fig. S1(a)).†

The powder XRD was performed to confirm the structure of nanoparticles. The *d*-spacing, determined by the deconvolution of a specific diffraction peak in the XRD pattern following Vegard's law, predicts a linear relationship between the crystal lattice parameter and the concentration of the constituent elements.[17,18] As shown in Fig. 2(a), the diffraction peaks of Ag (111), (200), (220), and (311) planes of Ag NPs were located at $2\theta = 38°$, 45°, 64°, and 77°, respectively. These distinct peaks are the structural features of Ag NPs, which also appear in the XRD pattern of Ag···AzoPy and Ag···Br–Br···AzoPy nanoparticles,

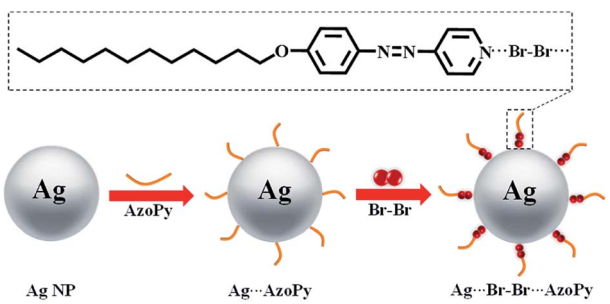


Scheme 1 Schematic illustration of organic–inorganic hybrid liquid crystals (Ag···Br–Br···AzoPy).

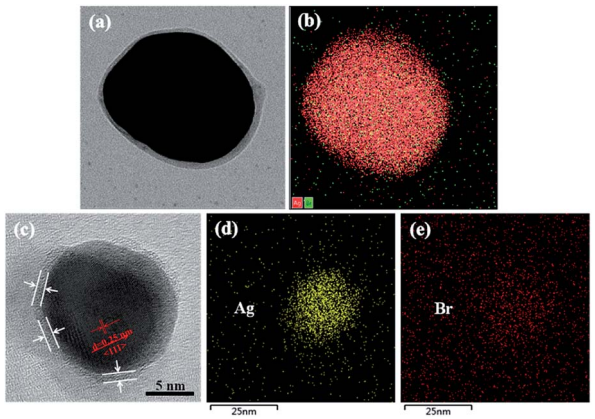


Fig. 1 The STEM image (a), EDS Ag and Br elemental mapping image (b), and HR-TEM image (c) of the di-noncovalent bonded Ag···Br–Br···AzoPy nanoparticle compared to EDS elemental mapping images of Ag (d) and Br (e). Mapping of the Ag region is depicted in yellow, while the Br region is shown in red.

confirming the successful formation of organic–inorganic hybrid complexes of Ag NPs.[19–21]

The UV-vis absorption spectra of Ag NPs, AzoPy, Ag···AzoPy nanoparticles, Br–Br···AzoPy, and Ag···Br–Br···AzoPy nanoparticles in acetone are shown in Fig. 2(b). The surface plasmon resonance (SPR) band of pristine Ag NPs is barely detectable because of the insolubility of Ag NPs in acetone. The absorption maximum ($\lambda_{max}$) of AzoPy and Ag···AzoPy nanoparticles are located in the same band at 352 nm, and the SPR band of Ag in Ag···AzoPy nanoparticles is absent because of the weak interaction between the electronic doublet of the nitrogen atom of the pyridyl moiety and the Ag surface.[22–24] However, compared to the Br–Br···AzoPy, the Ag···Br–Br···AzoPy nanoparticles showed a large redshift with $\lambda_{max}$ at 393 nm because of the incorporation of Ag NPs to AzoPy, demonstrating a stronger interaction of Br–Br···AzoPy with Ag NPs than with Ag···AzoPy nanoparticles, leading to the formation of the Ag···Br non-covalent bond composites.

In addition, the UV-vis absorption spectra of Ag···Br–Br···AzoPy nanoparticles at different concentrations of Ag NPs in acetone and a mixture of surface-stabilised Ag NPs and the AzoPy ligand in the solution were evaluated (Fig. S2†).

Further investigation of the Ag···Br–Br···AzoPy nanoparticles was corroborated by the Raman spectra. The Raman spectra of Ag···AzoPy nanoparticles showed a strong band at 249 $cm^{-1}$, characteristic of adsorbed pyridine groups compared to AzoPy (Fig. 2(c)), which is similar in frequency to the strong bands reported for pyridine adsorbed on Ag electrodes[25] and Ag sols.[26] However, the selective Raman enhancement by excitation at 785 nm was observed, corresponding to the characteristic Ag···Br vibrations at 151.8 $cm^{-1}$ in Ag···Br–Br···AzoPy nanoparticles, which is a result of the complexation between halogen-bonded azodye molecules Br–Br···AzoPy and Ag NPs after adding $Br_2$ to Ag···AzoPy nanoparticles.

This extraordinary enhancement was caused by the metal–molecule interaction, which involves the exchange mixing of Ag

 This journal is © The Royal Society of Chemistry 2020

Open Access Article. Published on 30 September 2020. Downloaded on 7/18/2025 9:02:30 PM.
This article is licensed under a Creative Commons Attribution-NonCommercial 3.0 Unported Licence.

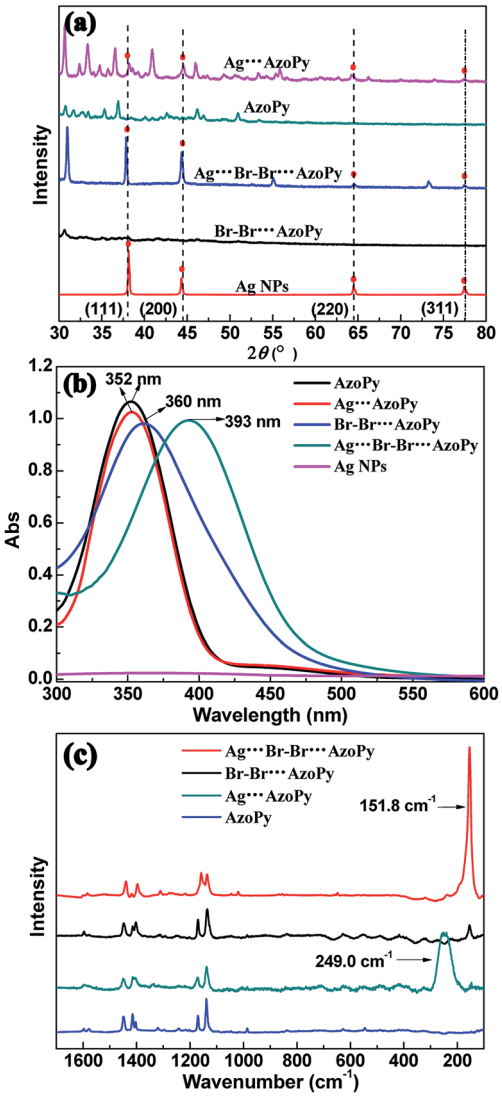


Fig. 2 The X-ray diffraction patterns (a), UV-vis absorption spectra of Ag NPs, AzoPy, Ag···AzoPy, Br–Br···AzoPy, and Ag···Br–Br···AzoPy in acetone (dashed line: predicted diffraction peaks for Ag metal) (b), and the Raman spectra of AzoPy, Br–Br···AzoPy, Ag···AzoPy, and Ag···Br–Br···AzoPy nanoparticles in the solid state (c).

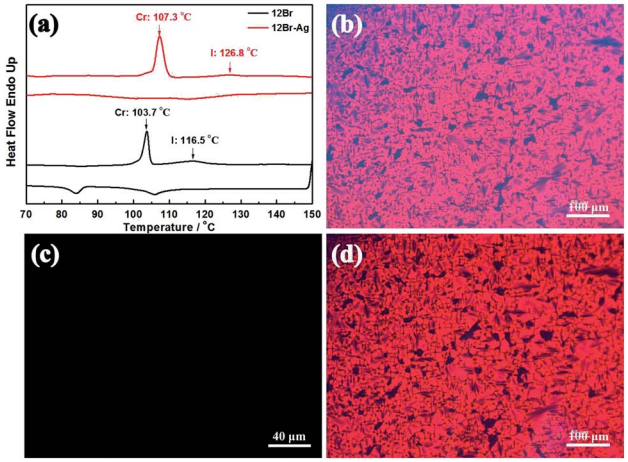


Fig. 3 The DSC measurements of composites 12Br and 12Br–Ag in heating and cooling cycle (a), POM images of 12Br–Ag at 120 °C on cooling from the isotropic phase (b), in vertical orientation cell in liquid crystal temperature (c), and upon UV irradiation (d).

electron–hole pairs and the HOMO–LUMO excited state of bromine molecules.[27,28] These results confirm that Ag···Br–Br···AzoPy nanoparticles were successfully assembled based on the interaction of $Br_2$ with the N atom of the pyridyl moiety by bromine bonding and the surface of Ag NPs by the electrostatic interaction. Furthermore, the XPS and $^1$H NMR spectra were recorded to further ascertain the bonding between Br–Br···AzoPy ligand molecules and Ag NPs (Fig. S3–S5†)

Fig. 3(a) shows the mesophase produced by the organic–inorganic hybrid complexes *via* the *in situ* synthesis of Ag NPs in AzoPy, and then linked by the halogen bonding, which stabilised the mesophase with an increase of 10.3 °C in the liquid crystal to isotropic transition compared with 12Br in heating cycle owing to the chemisorption of mesogens on nanoparticles.[29] This is different from the physical mixture of liquid crystals and nanoparticle hybrid systems, which lower the temperature (destabilisation) of the liquid crystal phases with the metal nanoparticles. The POM images of 12Br–Ag show focal conic fan textures between plain glass slides (Fig. 3(b)) and a uniform dark image in a vertical-orientation cell at their liquid crystal temperatures (Fig. 3(c)), which is similar to the smectic A phase of the pristine materials (12Br).[8] However, the photochemical phase transition in 12Br–Ag induced by UV irradiation was unlike that of the previously reported[8] brominated compounds (12Br; Fig. 3(d)).

After the annealing process, the SAXS experiments were employed to confirm the type of the smectic mesophase, as shown in Fig. 4. Two peaks with q values of 1.36 and 2.78 nm$^{-1}$ were detected for 12Br–Ag, similar to those observed for 12Br. The ratio of the scattering vectors of these two peaks was 1 : 2, indicating a smectic packing of 12Br–Ag. Using the MM2 force field method, it was determined that the *d*-spacings of the first diffraction peaks of 12Br and 12Br–Ag were 5.10 and 4.64 nm approximately, which is 1.67 and 1.41 times the length of the

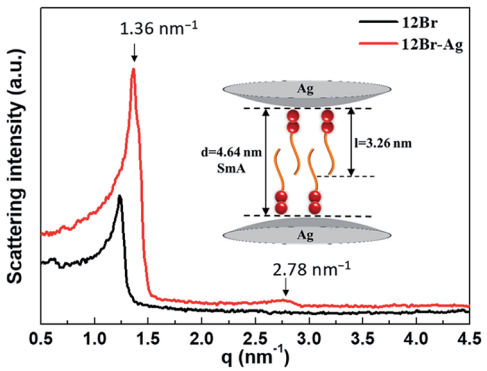


Fig. 4 The SAXS patterns of 12Br and 12Br–Ag after the annealing process with intensity in log scale. The inset picture is the schematic drawing of the smectic packing of 12Br–Ag.

Open Access Article. Published on 30 September 2020. Downloaded on 7/18/2025 9:02:30 PM.
This article is licensed under a Creative Commons Attribution-NonCommercial 3.0 Unported Licence.

calculated molecular 12Br ($l = 3.06$ nm) and 12Br–Ag complexes ($l = 3.26$ nm, the length includes the non-interaction distance between the peripheral bromine atom and the Ag NPs), respectively. Thus, the structures of 12Br and 12Br–Ag could be interdigitated smectic A phase, in which parts of the 12Br–Ag molecules overlap (see the inset picture in Fig. 4). The $d/l$ ratio of 12Br–Ag decreases compared to that of 12Br, probably because of the distinct electronic properties between them, which were induced by the *in situ* synthesis of Ag NPs in AzoPy.

The directing abilities of the Ag NPs are selective to surpass those of the alignment layers of the cell according to the temperature condition, which implies that doping with Ag NPs in the liquid crystal plays a dominant role in changing the birefringence by decreasing the *d*-spacing and inhibiting the orientation, as shown in Fig. S6 and S7.†

Furthermore, when dyes are localised near either free or immobilised metal particles, their luminescence (*i.e.*, fluorescence) intensifies, which is known as metal-enhanced fluorescence (MEF).[30–32] To investigate the occurrence and intensification of MEF in AzoPy, the fluorescence emission of the free AzoPy ligands and their corresponding complexes with Ag NPs were evaluated, as shown in Fig. S8(a).† It is important to note that the fluorescence intensity of Ag···Br–Br···AzoPy nanoparticles was approximately three times higher than that of Ag···AzoPy nanoparticles. This implies that the insertion of $Br_2$ between the AzoPy ligand and Ag nanoparticles intensifies the MEF of the ligand. This interesting characteristic is attributed to the increased distance between the azodye molecule and the Ag NP surface due to the presence of the intervening $Br_2$. As shown in Fig. S9,† the MM2 molecular mechanics calculations support this hypothesis.

The influence of the concentration of Ag NPs, different excitation wavelengths, and doping method on the fluorescence enhancement effect was evaluated in detail (Fig. S8(b–d) and S10†). The fluorescence quantum yield and fluorescence lifetime of the azodye functionalised Ag NPs were determined, as shown in Fig. S11, S12 and Table S1.†

To investigate the viability of halogen-bonded liquid crystals for application as sensors in metal pollution, inspired by the above-mentioned intensification phenomenon of the MEF and SERS of the organic and inorganic hybrid liquid crystal, 12Br was used for detecting silver components under realistic conditions, such as liquid waste produced in the preparation of conductive silver ink and tap water. As shown in Fig. 5(a), the diffraction peaks of Ag (200), (220), and (311) planes of Ag NPs in liquid waste are located at 45°, 64°, and 74°, respectively; thus, recovering silver from the waste liquid. Thereafter, trace amounts of silver were further detected in tap water. Although the content of silver in the tap water was extremely low, the detection signals of the Ag (111) and (200) planes at $2\theta = 38°$ and 45° could also be detected by 12Br due to the interaction between 12Br and silver in water with high sensitivity.

In addition to XRD characterisation, we studied the detection of silver in liquid waste and tap water *via* Raman spectroscopy. Compared to 12Br–Ag, the Raman peak of the bromine stretching vibration frequency of 12Br appeared at 222.4 $cm^{-1}$ and 166.8 $cm^{-1}$, but no SERS signals were detected because of weak interaction obtained by mixing them directly, as shown in Fig. 5(b). Instead, the N=N stretching and azobenzene quadrant stretching at 1414 $cm^{-1}$ and 1452 $cm^{-1}$ became active due to the interaction of the azobenzene ring and N atom with silver. These results confirm that the 12Br halogen-bonded liquid crystal is capable of detecting silver in a water environment and has the potential to transform metal pollution into valuable organic–inorganic hybrid mesogenic materials.

In conclusion, $Br_2$ was successfully introduced as a bridge between Ag NPs and the AzoPy ligand by electrostatic interaction and halogen bonding at the Ag NP surface and azodye end, respectively, thereby displaying liquid crystalline properties with the intensification of the MEF and SERS. The 12Br–Ag was difficult to orientate by the alignment layers of the cell in the liquid crystal temperature but could orientate after the annealing treatment at room temperature. More importantly, the bromine-bonded complex was used as a sensor for detecting silver in aqueous fluids and was capable of transforming waste metal pollution into valuable organic–inorganic hybrid liquid crystals for potential ultrasensitive detection in the water-environment monitoring and analytical chemistry.

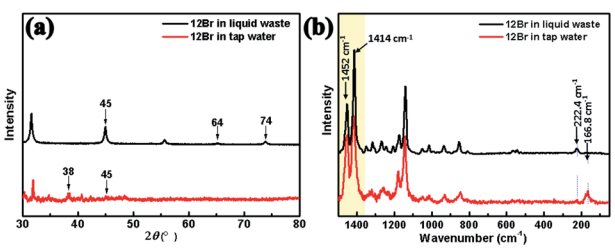


Fig. 5 The XRD pattern and Raman spectra of 12Br in liquid waste produced from the preparation of conductive silver ink and tap water (100 mg $mL^{-1}$), respectively.

## Conflicts of interest

There are no conflicts of interest to declare.

## Acknowledgements

This work was supported by the National Natural Science Foundation of China (grant no. 51702019, 51927806, 51773002, 21776021), National Key R&D Program of China (2018YFB0703702), Beijing Municipal Excellent Talents Foundation (grant no. 2017000020124G080), Science and Technology Planning Project of 2020 Beijing Education Commission (KM202010015006).

## Notes and references

1 (*a*) A. Priimagi, G. Cavallo and A. Forni, *Adv. Funct. Mater.*, 2012, **22**, 2572; (*b*) A. Priimagi, G. Cavallo, P. Metrangolo and G. Resnati, *Acc. Chem. Res.*, 2013, **46**, 2686.
2 H. M. D. Bandara and S. C. Burdette, *Chem. Soc. Rev.*, 2012, **41**, 1809–1825.

 This journal is © The Royal Society of Chemistry 2020

Open Access Article. Published on 30 September 2020. Downloaded on 7/18/2025 9:02:30 PM.
This article is licensed under a Creative Commons Attribution-NonCommercial 3.0 Unported Licence.

3 Y. Chen, H. Yu, M. Quan, L. Zhang, H. Yang and Y. Lu, *RSC Adv.*, 2015, **5**, 4675–4680.
4 Y. Chen, M. Quan, H. Yu, L. Zhang, H. Yang and Y. Lu, *RSC Adv.*, 2015, **5**, 31219–31225.
5 H. Zhang, R. Hao, J. K. Jackson, M. Chiao and H. Yu, *Chem. Commun.*, 2014, **50**, 14843–14846.
6 A. Priimagi, M. Saccone, G. Cavallo, A. Shishido, T. Pilati, P. Metrangolo and G. Resnati, *Adv. Mater.*, 2012, **24**, OP345–OP352.
7 M. Du, L. Li, J. Zhang, K. Li, M. Cao, L. Mo, G. Hu, Y. Chen, H. Yu and H. Yang, *Liq. Cryst.*, 2019, **46**, 37–44.
8 Y. Chen, H. Yu, L. Zhang, H. Yang and Y. Lu, *Chem. Commun.*, 2014, **50**, 9647–9649.
9 R. Klajn, K. P. Browne, S. Soh and B. A. Grzybowski, *Small*, 2010, **6**, 1385–1387.
10 R. Klajn, P. J. Wesson and K. J. M. Bishop, *Angew. Chem., Int. Ed.*, 2009, **48**, 7035–7039.
11 T. Ely, S. Das, W. Li, P. Kundu, E. Tirosh, D. Cahen, A. Vilan and R. Klajn, *Synlett*, 2013, **24**, 2370–2374.
12 S. Das, P. Ranjan, P. S. Maiti, G. Singh and R. Klajn, *Adv. Mater.*, 2013, **25**, 422–426.
13 (*a*) J. Duan, M. Wang, H. Bian, Y. Zhou, J. Ma, C. Liu and D. Chen, *Mater. Chem. Phys.*, 2014, **148**, 1013–1021; (*b*) T. K. Biswas, S. M. Sarkar, M. M. Yusoff and M. L. Rahman, *J. Nanoelectron. Optoelectron.*, 2018, **13**, 378–386; (*c*) J. F. Duan, J. Ma, B. Wu and Q. Li, *J. Mater. Chem. C*, 2014, **13**, 2375–2386.
14 R. Klajn, *Pure Appl. Chem.*, 2010, **82**, 2247–2279.
15 J. H. Ding and D. L. Gin, *Chem. Mater.*, 2000, **12**, 22–24.
16 A. Haryono and W. H. Binder, *Small*, 2006, **2**, 600–611.
17 I. K. Shim, Y. I. Lee, K. J. Lee and J. Joung, *Mater. Chem. Phys.*, 2008, **110**, 316–321.
18 X. Yuan, G. Sun, H. Asakura, T. Tanaka, X. Chen, Y. Yuan and N. Yan, *Chem.–Eur. J.*, 2013, **19**, 1227–1234.
19 Z. P. Zhang, L. D. Zhang, S. X. Wang, W. Chen and Y. Lei, *Polymer*, 2001, **42**, 8315–8318.
20 T. K. Sarma, D. Chowdhury, A. Paul and A. Chattopadhyay, *Chem. Commun.*, 2002, **10**, 1048–1049.
21 X. M. Yang and Y. Lu, *Mater. Lett.*, 2005, **59**, 2484–2487.
22 P. K. Jain, S. Eustis and M. A. El-Sayed, *J. Phys. Chem. B*, 2006, **110**, 18243–18253.
23 Z. Sun, W. Ni, Z. Yang, X. Kou, L. Li and J. Wang, *Small*, 2008, **4**, 1287–1292.
24 K. Liu, A. Ahmed, S. Chung, K. Sugikawa, G. Wu, Z. Nie and E. Kumacheva, *ACS Nano*, 2013, **7**, 5901–5910.
25 J. A. Creighton, C. G. Blatchford and M. G. Albrecht, *J. Chem. Soc., Faraday Trans.*, 1979, **75**, 790–798.
26 J. A. Creighton, M. G. Albrecht, R. E. Hester and J. A. D. Matthew, *Chem. Phys. Lett.*, 1978, **55**, 55–58.
27 H. Wetzel, H. Gerischer and B. Pettinger, *Chem. Phys. Lett.*, 1981, **78**, 392–397.
28 A. M. Michaels, J. Jiang and L. Brus, *J. Phys. Chem. B*, 2000, **104**, 11965–11971.
29 M. Mitov, C. Portet, C. Bourgerette, E. Snoeck and M. Verelst, *Nat. Mater.*, 2002, **1**, 229–231.
30 K. H. Drexhage, *Prog. Opt.*, 1974, **12**, 163–232.
31 J. Zhang and J. R. Lakowicz, *J. Phys. Chem. B*, 2005, **109**, 8701–8706.
32 C. R. Mayer, E. Dumas and F. Sécheresse, *Chem. Commun.*, 2005, **3**, 345–347.